

Disentangling the global multiplicity and spectral shape fluctuations in radial flow

Somadutta Bhatta,¹ Aman Dimri,¹ and Jiangyong Jia^{1,2,*}

¹*Department of Chemistry, Stony Brook University, Stony Brook, NY 11794, USA*

²*Physics Department, Brookhaven National Laboratory, Upton, NY 11976, USA*

(Dated: April 29, 2025)

Radial flow is a key collective phenomenon in heavy-ion collisions, manifests through event-by-event fluctuations in transverse momentum (p_T) spectra. The p_T -differential radial flow, $v_0(p_T)$, initially conceived to capture local spectral shape fluctuations, is influenced by global multiplicity fluctuations. Using the HIJING model, we explore how different definitions of event activity for centrality and spectral normalization schemes affect $v_0(p_T)$. We find these methodological variations induce a constant offset in $v_0(p_T)$ without altering its shape, indicating that the dynamic p_T -differential information on radial flow remains robust, but its absolute magnitude is meaningful only up to a baseline offset dictated by global multiplicity fluctuations.

Introduction. Radial and anisotropic flows are critical indicators of collective behavior in quark-gluon plasma (QGP) formed during high-energy heavy-ion collisions [1]. While anisotropic flow (v_n , $n = 1, 2, \dots$) has been studied extensively, radial flow (v_0), originating from initial energy density variations and driven by pressure gradients, remains relatively underexplored. Event-by-event (EbE) fluctuations in the overall system size and local densities cause radial flow and resultant transverse momentum (p_T) spectra, $N(p_T) = dN/dp_T$, to vary from event to event [2, 3]. Consequently, radial flow fluctuations provide valuable insights into QGP properties, including its equation of state, shear and bulk viscosities [4–6].

Historically, radial flow studies have focused primarily on integral quantities such as the average transverse momentum $[p_T]_R$ or the particle multiplicity N_R within a momentum range R . Radial flow fluctuations are accessed using multi-particle correlations, $c_0\{k\}$ and $v_0\{k\}$ ($k = 1, 2, \dots$), formulated analogously to anisotropic flow:

$$\begin{aligned} c_{0,x}\{1\} &= v_{0,x}\{1\} = \langle x \rangle, \\ c_{0,x}\{2\} &= v_{0,x}\{2\}^2 = \langle (\delta x)^2 \rangle / \langle x \rangle^2, \\ c_{0,x}\{3\} &= v_{0,x}\{3\}^3 = \langle (\delta x)^3 \rangle / \langle x \rangle^3, \\ c_{0,x}\{4\} &= v_{0,x}\{4\}^4 = \frac{\langle (\delta x)^4 \rangle - 3 \langle (\delta x)^2 \rangle^2}{\langle x \rangle^4}, \\ &\dots \end{aligned} \quad (1)$$

where $x = N_R$ or $[p_T]_R$, and $\delta x = x - \langle x \rangle$. For simplicity, we will use $v_0\{k\}$ for $x = N_R$ and $v_{0,p}\{k\}$ for $x = [p_T]_R$.

The majority of earlier measurements focused on the mean and variance of $[p_T]_R$, corresponding respectively to $v_{0,p}\{1\}$ and $v_{0,p}\{2\}$, although investigations into higher-order cumulants have recently begun [6–11]. Results from these integrated quantities demonstrated strong sensitivities to both the initial-state geometry

and the final-state properties of the QGP. Recent differential measurements by the ATLAS and ALICE experiments have advanced this field by studying two-particle radial flow fluctuations as functions of p_T or pseudorapidity η [12, 13]. These differential measurements allow rigorous tests of factorization relations [12] such as $c_0\{2\}(p_{T1}, p_{T2}) = v_0\{2\}(p_{T1})v_0\{2\}(p_{T2})$ and $c_0\{2\}(\eta_1, \eta_2) = v_0\{2\}(\eta_1)v_0\{2\}(\eta_2)$, directly confirming the collective nature of radial flow. Moreover, the p_T -dependent shape of $v_0\{2\}(p_T)$ was identified as uniquely sensitive to bulk viscosity. This work focuses exclusively on $v_0\{2\}(p_T)$, hereafter simplified as $v_0(p_T)$.

Spectral shape fluctuations and $v_0(p_T)$. Information about radial flow is embedded in the p_T -dependent yield in each event, $N(p_T)$, which can be decomposed into the product of the global multiplicity $N = \int N(p_T)dp_T$, and the normalized (fractional) spectrum, $n(p_T)$, such that $N(p_T) = Nn(p_T)$. Events exhibiting stronger (weaker) radial flow tend to display a flatter (steeper) $N(p_T)$ distribution (see top of Fig. 1). Such EbE fluctuations in $N(p_T)$ can be expressed through a decomposition into three terms (This view is consistent with the decomposition based on principal component analysis [14, 15]):

$$\delta N(p_T) = \langle n(p_T) \rangle \delta N + \langle N \rangle \delta n(p_T) + \delta N \delta n(p_T). \quad (2)$$

In most cases, the higher-order term $\delta N \delta n(p_T)$ is negligible. Variations in global multiplicity N are often associated with centrality dependence, whereas fluctuations in $n(p_T)$ reflect to genuine radial flow fluctuations. Although this separation is inherently ambiguous, it provides a useful framework for understanding the interplay between global multiplicity and radial flow fluctuations.

Radial flow information is extracted from the covariance between the local normalized spectrum $n(p_T)$ and $[p_T]$, often expressed in a factorizable form [16]:

$$\frac{\langle \delta n(p_T) \delta [p_T] \rangle}{\langle n(p_T) \rangle \langle [p_T] \rangle} = v_0(p_T) v_{0,p}, \quad (3)$$

where $v_{0,p} = \sqrt{\langle (\delta p_T)^2 \rangle_A} / \langle p_T \rangle_A$ is measured within a reference p_T range, $p_T^{\text{ref}} \in A$, and we note in the passing that

*Correspond to jiangyong.jia@stonybrook.edu

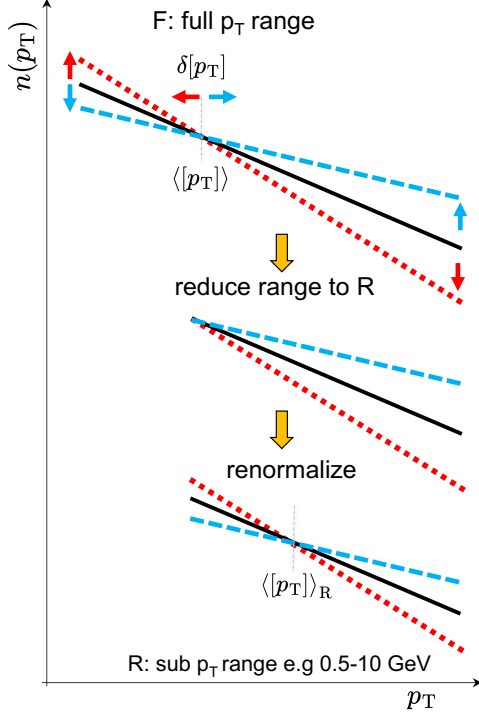


FIG. 1: Top: Schematic illustration showing how radial flow fluctuations create correlations between the EBe p_T -differential yield $n(p_T)$ and the EBe average transverse momentum $[p_T]$. The blue curve represents an event with larger-than-average radial flow, the red curve represents an event with smaller-than-average radial flow, and the black curve represents the ensemble-averaged spectrum. The zero-crossing point of $v_0(p_T)$, approximately at $\langle [p_T] \rangle$, depends on the normalization range chosen to obtain $n(p_T)$. Top-to-bottom: Fractional spectra obtained over a wider range F and its subrange R are normalized differently. Therefore, the spectral fluctuation in range R can be decomposed into a total multiplicity fluctuation term and a reduced spectral shape fluctuation term (Eq. (8)).

$v_0\{1\}(p_T) = \langle n(p_T) \rangle$ according to Eq. 1. ATLAS measurement indicates that $v_0(p_T)$ remains independent of the choice of p_T^{ref} [12]. Experimentally observed $v_0(p_T)$ displays characteristic behavior: it begins negative at low p_T , increases up to about 4 GeV while crossing zero at around $p_T = p_T^0 \approx \langle [p_T] \rangle$, and subsequently decreases at higher p_T . This rise and fall behavior potentially reflects the transition from a hydrodynamic flow-dominated region to a jet-quenching-dominated region.

The connection between $v_0(p_T)$ and local spectral shape fluctuations can be explicitly formulated as:

$$v_0(p_T) = \rho(n(p_T), [p_T]) \frac{\sqrt{\langle (\delta n(p_T))^2 \rangle}}{\langle n(p_T) \rangle}, \quad (4)$$

where $\rho(x, y) = \langle \delta x \delta y \rangle / \sqrt{\langle (\delta x)^2 \rangle \langle (\delta y)^2 \rangle} \in [-1, 1]$ represents the Pearson correlation coefficient between x and y , determining the sign of $v_0(p_T)$. Because $|v_0(p_T)| \leq \frac{\sqrt{\langle (\delta n(p_T))^2 \rangle}}{\langle n(p_T) \rangle}$, $v_0(p_T)$ captures only the portion

of the spectral fluctuation that is correlated with $[p_T]$. This correlation can be reduced by decorrelation effects between spectral fluctuations at high p_T and the $[p_T]$ fluctuations measured at low p_T .

Global multiplicity fluctuation cannot be eliminated. Ideally, the fractional spectrum $n(p_T)$ should be defined using all particles across the full transverse momentum range. However, experimental constraints typically limit measurements to charged particles within a restricted p_T range, denoted as “ R ”. The fractional spectrum defined with this restricted range, $n_R(p_T)$, retains the shape of $n(p_T)$ but is rescaled: $n_R(p_T) = n(p_T)N/N_R$. Even if the total multiplicity N remains fixed, the multiplicity within the restricted range, $N_R = \int_R N(p_T) dp_T$, can fluctuate statistically. This renormalization-induced fluctuation leads to a shift in the zero-crossing point of $v_0(p_T)$ from $p_T^0 \approx \langle [p_T] \rangle$ to $p_T^0 \approx \langle [p_T] \rangle_R$ (see Fig. 1). It is crucial to recognize that this shift is entirely due to the renormalization procedure and does not affect the factorization property (Eq. (3)), which remains valid for varying the p_T^{ref} used in the calculation of $v_{0,p}$.

The separation between global and local fluctuations thus is not uniquely defined. To further elucidate this, consider an alternative definition of the p_T -differential radial flow using the absolute spectrum $N(p_T)$:

$$\frac{\langle \delta N(p_T) \delta [p_T] \rangle}{\langle N(p_T) \rangle \langle [p_T] \rangle} = v'_0(p_T) v_{0,p}. \quad (5)$$

Substituting Eq. (2) and utilizing the approximation $\langle N(p_T) \rangle = \langle N n(p_T) \rangle = \langle N \rangle \langle n(p_T) \rangle (1 + \tau) \approx \langle N \rangle \langle n(p_T) \rangle$ (assuming the correlation term $\tau(p_T) = \frac{\langle \delta N \delta n(p_T) \rangle}{\langle N \rangle \langle n(p_T) \rangle}$ is negligible), we expect:

$$\Delta v_0 \equiv v'_0(p_T) - v_0(p_T) \quad (6)$$

$$\approx \frac{\langle \delta N \delta [p_T] \rangle}{\langle N \rangle \sqrt{\langle (\delta [p_T])^2 \rangle}} = \rho(N, [p_T]) \frac{\sqrt{\langle (\delta N)^2 \rangle}}{\langle N \rangle}. \quad (7)$$

This result demonstrates that the difference between the two definitions of $v_0(p_T)$ is a constant offset, directly proportional to the global multiplicity fluctuations and their correlation with the average transverse momentum. The sign of this offset is determined by the covariance between the total multiplicity and $[p_T]$, which is sensitive to the specific event class definitions employed.

The aforementioned difference arises from the inherent variations in N_R at constant N (as depicted in Fig. 1). Within the restricted p_T range R , the normalized spectrum is $n_R(p_T) = N(p_T)/N_R$. Consequently, fluctuations in $N(p_T)$ within this range can be approximated as:

$$\delta N(p_T) \approx \delta N_R \langle n_R(p_T) \rangle + \langle N_R \rangle \delta n_R(p_T). \quad (8)$$

Under the assumption that particles are independently sampled from the underlying momentum distribution, the fluctuation of N_R , being a subset of N , follows a binomial distribution with a sampling probability $\epsilon =$

$\langle N_R \rangle / \langle N \rangle$. Applying Eq. (7), the $v_0(p_T)$ calculated within the restricted range R , denoted as $v_{0,R}(p_T)$, differs from that calculated over the full p_T range, $v_0(p_T)$, by an offset:

$$\Delta v_{0,R} = v_{0,R}(p_T) - v_0(p_T) \quad (9)$$

$$\approx \rho(N, [p_T]) \frac{\sqrt{\langle (\delta N)^2 \rangle}}{\langle N \rangle} - \rho(N_R, [p_T]) \frac{\sqrt{\langle (\delta N_R)^2 \rangle}}{\langle N_R \rangle} \quad (10)$$

$$\approx - \left(\rho(N_R, [p_T]) \frac{\sqrt{\langle (\delta N_R)^2 \rangle}}{\langle N_R \rangle} \right)_N \quad (11)$$

$$= - \left(\rho(N_R, [p_T]) \sqrt{\frac{(1-\epsilon)}{N_R}} \right)_N. \quad (12)$$

The subscript N signifies that the quantities in the parenthesis are evaluated under the condition of fixed N . The approximation from Eq. (10) to Eq. (11) is valid because a change in the N is expected to induce a proportional change in the multiplicity within the subrange N_R .

Model setup. The interplay between global multiplicity fluctuation and spectral shape fluctuation is encoded in the Pearson correlation coefficient $\rho(N, [p_T])$. We investigate this interplay using the HIJING model [17], which simulates particle production as a superposition of independent $p + p$ collisions. The absence of genuine radial flow and the presence of high- p_T particles from hard-scattered jets also provide an ideal framework to study the non-flow baseline of $v_0(p_T)$.

We generate Pb+Pb collisions at $\sqrt{s_{NN}} = 5.02$ TeV, with a hard scale of 2 GeV (parameter HIPR1(10)=2). Charged particles with $|\eta| < 2.5$ and $p_T < 10$ GeV are selected for correlation analysis. These particles are divided into two subevents in η : $-2.5 < \eta_a < -\frac{\eta_{\text{gap}}}{2}$ and $\frac{\eta_{\text{gap}}}{2} < \eta_b < 2.5$. Two gap sizes, $\eta_{\text{gap}} = 0$ and 3, are used to evaluate the effects of short-range non-flow correlations and multiplicity fluctuations. The $[p_T]$ is calculated for reference particles in three p_T^{ref} ranges (0.5–2, 0.5–5 and 1–5 GeV), denoted by “A”, to study the effects of non-flow correlations. The $n(p_T)$ and $v_0(p_T)$ are calculated in three p_T ranges (0–10, 0.5–10 and 1–10 GeV) to investigate the impact of the relative multiplicity fluctuations within a subrange. We denote 0–10 GeV as the full range and 0.5–10 and 1–10 GeV as the subranges “R”. Events are classified based on charged particle multiplicity in various η ranges and the number of participating nucleons (N_{part}), as listed in Table I.

$n(p_T)$ or $N(p_T)$	p_T^{ref} (GeV)	Event activity
0–10 GeV, $ \eta < 2.5$	0.5–2	N_{ch} in $ \eta < 2.5$
0.5–10 GeV, $ \eta < 2.5$	0.5–5	N_{ch} in $2.5 < \eta < 3.2$
1–10 GeV, $ \eta < 2.5$	1–5	N_{ch} in $3.2 < \eta < 4$
		N_{ch} in $4 < \eta < 5$
		N_{part}

TABLE I: Selection of particles used for $n(p_T)$ or $N(p_T)$, for calculation of $[p_T]$, and for event activity classifications.

For each subevent, we calculate $[p_T]$, $N(p_T)$, and $n(p_T)$. The two-particle observables are calculated in narrow ranges of event activity estimators as: $\langle (\delta[p_T])^2 \rangle = \langle \delta[p_T]_a \delta[p_T]_b \rangle$, $\langle \delta n(p_T) \delta[p_T] \rangle = \frac{1}{2} \langle \delta n_a(p_T) \delta[p_T]_b + \delta n_b(p_T) \delta[p_T]_a \rangle$. The shift term in Eq. (7) and Eq. (10) is also estimated using the two-subevent method:

$$\Delta v_0 = \frac{\langle \delta N_a \delta[p_T]_b \rangle}{\langle N_a \rangle \sqrt{\delta[p_T]_a \delta[p_T]_b}} \quad (13)$$

Our analysis procedure is consistent with the choice used in the ATLAS measurement.

Particle production in HIJING is based on the idea of independent sources. If the particles used for event activity selection are independent of those used in the analysis, various two-subevent quantities involved in Eq. (13) are expected to follow simple power-law behavior with the number of sources N_s :

$$\begin{aligned} \langle \delta N_a \delta N_b \rangle &\propto N_s \\ \langle \delta[p_T]_a \delta[p_T]_b \rangle &\propto 1/N_s \\ \sqrt{\langle \delta N_a \delta N_b \rangle} / \langle N_a \rangle &\propto 1/\sqrt{N_s} \\ \Delta v_0 &\propto 1/\sqrt{N_s} \\ \langle \delta N_a \delta[p_T]_b \rangle &\sim \text{const} \\ \sqrt{\langle \delta N_a \delta N_b \rangle} \sqrt{\langle \delta[p_T]_a \delta[p_T]_b \rangle} &\sim \text{const} \\ \rho(N_a, [p_T]_b) &\equiv \frac{\langle \delta N_a \delta[p_T]_b \rangle}{\sqrt{\langle \delta N_a \delta N_b \rangle} \sqrt{\langle \delta[p_T]_a \delta[p_T]_b \rangle}} \sim \text{const} \\ \sqrt{N_a} \Delta v_0 &\sim \text{const} \end{aligned} \quad (14)$$

Here, “const” represents the value of the respective

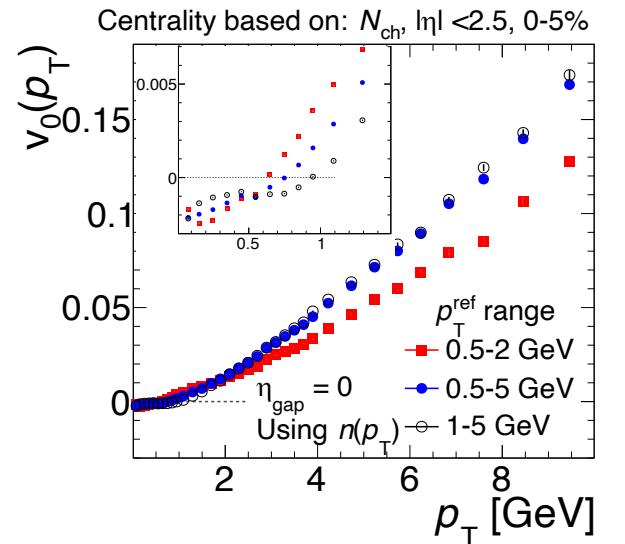


FIG. 2: The $v_0(p_T)$ calculated for fractional spectra in 0–10 GeV range (Eq. (3)) for three p_T^{ref} selections in 0–5% most central Pb+Pb collisions. The inset shows a zoomed-in view of the low p_T region.

observable determined by particle production within each

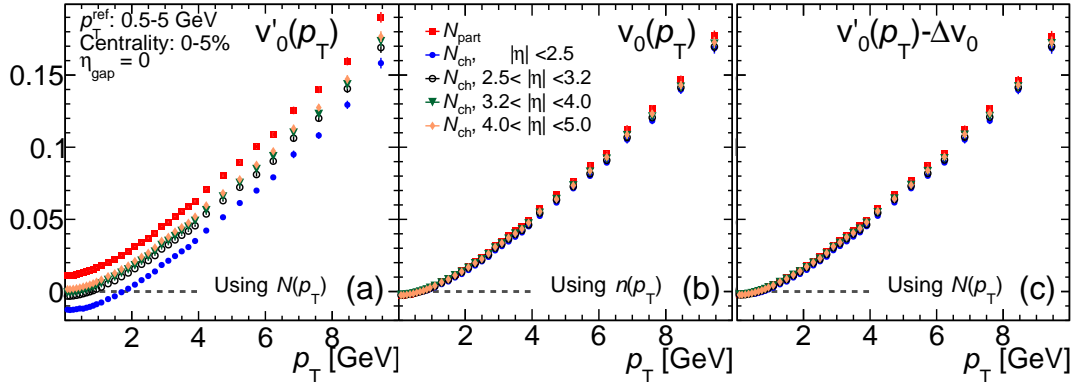


FIG. 3: The $v_0(p_T)$ obtained using $N(p_T)$ (left), $n(p_T)$ (middle), and $N(p_T)$ but applying the correction calculated via Eq. (7) in the two-subevent format Eq. (13) (right) for several event activity selections in 0–5% most central Pb+Pb collisions.

source (e.g., each $p + p$ collision), which should also be independent of centrality.

Results. *Impact of non-flow.* Figure 2 shows $v_0(p_T)$ calculated in the 0–10 GeV range using three p_T^{ref} selections in central collisions. Significant differences are observed at high p_T , as expected due to the dominance of non-flow correlations from jets and dijets. These differences extend into the low p_T region, as seen in the inset, where non-flow correlations also result in a variation of the zero-crossing point with the choice of p_T^{ref} . The magnitude of $v_0(p_T)$ is also much smaller than experimental data [12], supporting the interpretation that collective radial flow dominates the measurements.

Residual multiplicity fluctuation. Figure 3a displays results obtained using $N(p_T)$ via Eq. (5) for different event activity selections. These results show a similar increasing trend with p_T but exhibit significant vertical shifts among them. These event-activity-class-dependent shifts can drastically alter the values of p_T^0 , and for event classes based on N_{part} or N_{ch} in the forward rapidity, the obtained $v_0(p_T)$ never crosses zero, implying local spectra the fluctuations and overall multiplicity fluctuations are entangled. In contrast, results based on $n(p_T)$ in Fig. 3b cluster nicely together with a common zero-crossing point around the average transverse momentum of the inclusive spectra, implying that $v_0(p_T)$ obtained from fractional spectra is insensitive to the event class selection. Figure 3c demonstrates that the differences between Fig. 3a and Fig. 3b are largely accounted for by the Δv_0 correlation calculated using Eq. (7).

Figure 4a compares the actual difference $v'_0(p_T) - v_0(p_T)$ (points) with the predicted difference Δv_0 (dotted lines) as a function p_T . The $v'_0(p_T) - v_0(p_T)$ is nearly constant and is well reproduced by Δv_0 . Figure 4b compares the centrality dependence of $v'_0(p_T) - v_0(p_T)$ at $p_T = 1$ GeV (points) with the predicted Δv_0 (dotted lines), both scaled by $\sqrt{N_{\text{part}}}$. Again, they show remarkable agreement across the full centrality range.

These results indicate that the observable $v_0(p_T)$ provides a data-driven way to separate fluctuations in global

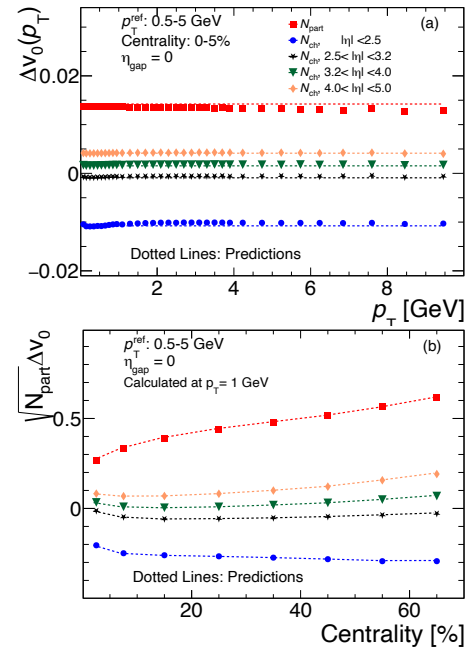


FIG. 4: Top: $v'_0(p_T) - v_0(p_T)$ (points) compared with Δv_0 estimated via Eq. (7) in its two-subevent format (dotted lines) in 0–5% most central Pb+Pb collisions. Bottom: Centrality dependence of $\sqrt{N_{\text{part}}}(v'_0(p_T) - v_0(p_T))$ at $p_T = 1$ GeV (points) compared with $\sqrt{N_{\text{part}}}\Delta v_0$ (dotted lines).

multiplicity and p_T -dependent spectral shape. This correction term increases with the η gap between the particles of interest and those used to define event activity, consistent with the behavior of multiplicity decorrelation $\frac{\langle \delta N(\eta_1) \delta N(\eta_2) \rangle}{\langle N(\eta_1) \rangle \langle N(\eta_2) \rangle}$ [18, 19] measured by ATLAS previously [20]. Some of these effects can be attributed to inherent longitudinal centrality decorrelation in the initial state of heavy-ion collisions [21], resulting from a combined effect of forward-backward fluctuations in the particle production profile associated with each source and the asymmetry in the number of participating nucle-

ons in the forward and backward directions.

Since the HIJING model is based on an independent source picture, various quantities involved in Δv_0 are expected to follow simple scaling laws described in Eq. (14). We explicitly verified three relations, $\langle \delta N_a \delta [p_T]_b \rangle$, $\rho(N_a, [p_T]_b)$ and $\sqrt{N_{\text{part}}} \Delta v_0$ in Figure 5. They are approximately constant or vary slowly with centrality.

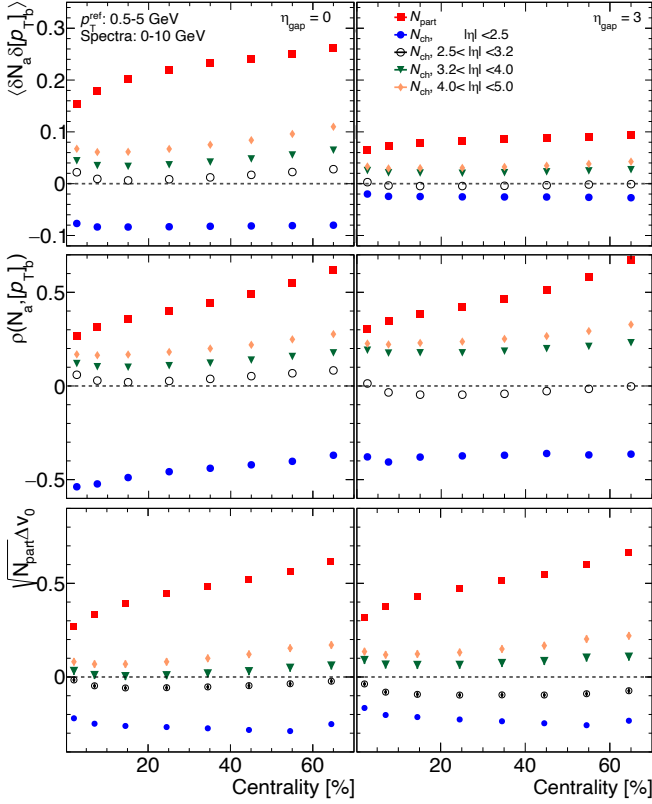


FIG. 5: The components of Δv_0 in Eq. (13), $\langle \delta N_a \delta [p_T]_b \rangle$ (top row), $\rho(N_a, [p_T]_b)$ (middle row) and $\sqrt{N_{\text{part}}} \Delta v_0$ (bottom row) for $\eta_{\text{gap}} = 0$ (left column) and $\eta_{\text{gap}} = 3$ (right column), calculated in 0–5% most central collisions, for various event activities classes.

One case in Figs. 4 and 5, however, warrants special attention. When particles used to define event activity strongly overlap with those used to calculate the observables (e.g. N_{ch} defined in $|\eta| < 2.5$, blue symbols), we observed negative values for these observables. The magnitudes of $\langle \delta N_a \delta [p_T]_b \rangle$ are nearly constant with centrality and are smaller for larger η_{gap} . This can be understood because the total multiplicity N_{ch} has contributions from the usual subevents a , b , and the middle subevent c , such that $N_{\text{ch}} = N_a + N_b + N_c$. A requirement of fixed N_{ch} results in anticorrelations between N_a , N_b , and N_c , described by a multinomial distribution. This anticorrelation is a statistical artifact without dynamical origin. When $\eta_{\text{gap}} = 0$, we have $N_c = 0$, and the anticorrelation is strongest between N_a and N_b (or $[p_T]_b$). As η_{gap} increases, more particles are included in subevent

c , reducing the anticorrelation between N_a and N_b (or $[p_T]_b$) (bottom row of Fig. 5). It is crucial to point out that this artifact only affects the $v'_0(p_T)$ but not $v_0(p_T)$.

When particles used to define event activity do not overlap with those used to calculate the observables, the correlations are close to zero or slightly positive. The correlation strength is larger for N_{ch} defined in more forward η and is strongest when N_{part} is used. The correlation also shows a significant increase toward more peripheral collisions when N_{part} is used for event selection. As mentioned earlier, these multiplicity and mean p_T correlations reflect the longitudinal dynamics present in the HIJING model.

Consequence of varying p_T acceptance. Lastly, we discuss a practical issue. Real experiments often have different acceptance coverage in p_T . For example, ALICE typically performs measurements for $p_T > 0.1$ GeV, CMS for $p_T > 0.3$ GeV, and ATLAS for $p_T > 0.5$ GeV in Pb+Pb collisions. The fractional spectra obtained in these ranges are normalized differently. According to Eq. (12), even if the total multiplicity N in the full acceptance is fixed, N_R in a subrange still fluctuates. This fluctuation leads to a downward shift that moves the p_T^0 to match the average transverse momentum in the range R . This expectation is confirmed in Fig. 6a, where measurements based on $n_R(p_T)$ depend on the p_T range of the spectra (left). A simple correlation based on Eq. (10) accounts for the differences among them, as shown in Figure 6b. It appears that the location of the zero-crossing point is purely a kinematic effect associated with the properties of the average spectra and does not reflect genuine dynamical radial flow fluctuations.

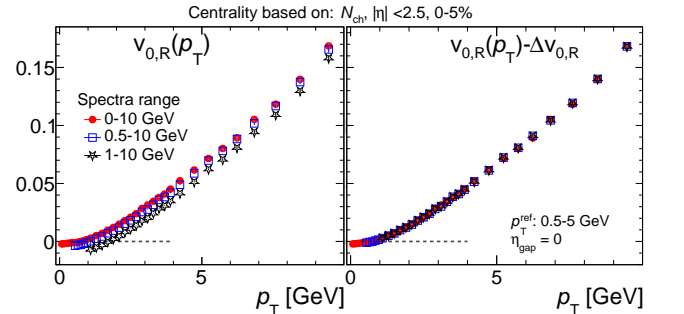


FIG. 6: Left: The $v_0(p_T)$ obtained using spectra normalized using $N_R = \int_a^b N(p_T) dp_T$, obtained in three p_T ranges, 0–10, 0.5–10 and 1–10 GeV, in 0–5% most central collisions. Right: The results obtained after correcting for the offset predicted using Eq. (10).

Summary Event-by-event fluctuations of final-particle particle spectrum $N(p_T)$ serve as a sensitive probe of the collective radial flow in the quark-gluon plasma. Experimentally, these fluctuations are accessed using the observable $v_0(p_T)$ (or $v'_0(p_T)$), which characterizes the correlation between the normalized spectrum $n(p_T)$ (or the original spectrum $N(p_T)$) and the event-by-event spectral shape, encoded in the average trans-

verse momentum $[p_T]$. These spectral fluctuations can be decomposed into contributions from global multiplicity fluctuations (δN , $N = \int N(p_T) dp_T$) and local spectral shape fluctuations ($\delta n(p_T)$, $n(p_T) = N(p_T)/N$):

$$\delta N(p_T) = \langle n(p_T) \rangle \delta N + \langle N \rangle \delta n(p_T) .$$

Using the HIJING model, we investigated the interplay between δN and $\delta n(p_T)$, and the impact of non-flow correlations on $v_0(p_T)$ using the HIJING model. The extracted $v_0(p_T)$ exhibits a monotonic increase with p_T and a strong dependence on the p_T range used to calculate $[p_T]$, consistent with the dominance of non-flow. We found that δN and hence $v'_0(p_T)$ are sensitive to the event activity variable used for centrality classification and is impacted by possible autocorrelation effects, while $v_0(p_T)$ is sensitive to the p_T range over which $n(p_T)$ is defined. However, all these different formulations are related by a constant offset reflecting variations in N and its correlation with $[p_T]$. Furthermore, the integrated $[p_T]$ fluctuations are insensitive to these offsets (see Appendix B). Therefore, we conclude that the dynamical differential information of $v_0(p_T)$ is meaningful only up to a constant baseline determined by global multiplicity fluctuations.

Appendix

We would like to relate the $v_0(p_T)$ calculated in different kinematic ranges. We consider the full range “ F ”, a range in a specific experiment, “ R ”, for example 0.5–10 GeV in ATLAS, and the reference p_T range “ A ” used to calculate the $[p_T]$ (see Figure 7). Quantities calculated F will not be labelled, while those calculated in the other cases will be labelled by subscript R or A . We use $N(p_T)$ and $n(p_T)$ to represent the particle yield and fractional yield at p_T , respectively, and use N to represent the total particle multiplicity. We use \int_A to represent an integration of p_T in the range A . The following aims to provide a coherent and consistent discussion, and it borrows heavily from Refs. [16, 22].

A. The observables in range A expressed using variables in the full range

The average transverse momentum in an event and its ensemble average in A is given

$$[p_T]_A = \frac{1}{N_A} \int_A p_T N(p_T) \quad (15)$$

$$\begin{aligned} \langle p_T \rangle_A &\equiv \langle [p_T] \rangle_A = \left\langle \frac{1}{N_A} \int_A p_T N(p_T) \right\rangle \\ &= \frac{1}{\langle N_A \rangle} \left[\int_A p_T \langle N(p_T) \rangle - \int_A p_T \langle n_A(p_T) \delta N_A \rangle \right] \\ &\approx \frac{1}{\langle N_A \rangle} \int_A p_T \langle N(p_T) \rangle \end{aligned} \quad (16)$$

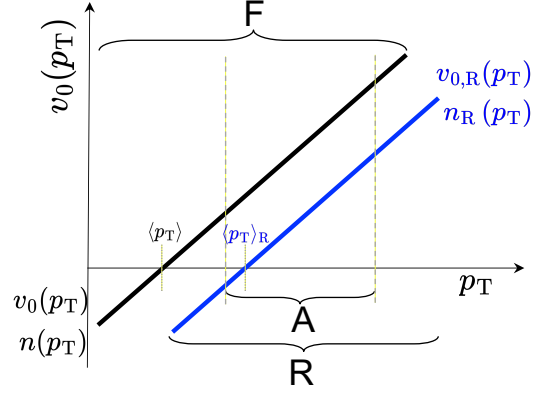


FIG. 7: The p_T -differential spectra shape fluctuation calculated in the range F , $v_0(p_T)$, and range R , $v_{0,R}(p_T)$. They differ by a constant vertical shift s , which is controlled by the difference between $\langle p_T \rangle$ and $\langle p_T \rangle_R$ (see main text). The range A is the reference p_T used to calculate the integral v_0 and for measuring $v_0(p_T)$ and $v_{0,R}(p_T)$.

Note that the integral involving $\langle n_A(p_T) \delta N_A \rangle$ is a higher-order term, corresponding to the correlated fluctuation of the spectral shape and integrated multiplicity. The other term represents per-particle average transverse momentum, i.e., if we calculate $\langle p_T \rangle$ on a per-track basis instead of per-event basis, then Eq. (16) would be exact. From these, we obtain,

$$\begin{aligned} \delta[p_T]_A &= \frac{1}{N_A} \int_A p_T \delta N(p_T) - \frac{\delta N_A}{N_A} \langle p_T \rangle_A \\ &= \frac{1}{N_A} \int_A (p_T - \langle p_T \rangle_A) \delta N(p_T) \end{aligned} \quad (17)$$

The appearance of $\langle p_T \rangle_A$ is critical, because it absorbs δN_A , i.e., the contribution from the fluctuation of N_A . In particular, since A is a subrange, N_A still fluctuates even if N is fixed.

It is more convenient to express observables in terms of fractional spectra. Using $N(p_T) = n(p_T)N = \delta n(p_T)N + \langle n \rangle N$, we have

$$\begin{aligned} \langle N(p_T) \rangle &= \langle N \rangle \langle n(p_T) \rangle + \langle \delta N \delta n(p_T) \rangle \\ \delta N(p_T) &= N \delta n(p_T) + \delta N n(p_T) - \langle \delta N \delta n(p_T) \rangle . \end{aligned} \quad (18)$$

Eq. (16) can be rewritten as,

$$\begin{aligned} \langle p_T \rangle_A &= \frac{\int_A p_T \langle N(p_T) \rangle}{\int_A \langle N(p_T) \rangle} = \frac{\langle N \rangle \int_A p_T \langle n(p_T) \rangle + \int_A p_T \langle \delta N \delta n(p_T) \rangle}{\langle N \rangle \int_A \langle n(p_T) \rangle + \int_A \langle \delta N \delta n(p_T) \rangle} \\ &\approx \frac{\int_A p_T \langle n(p_T) \rangle}{\int_A \langle n(p_T) \rangle} \left(1 + \frac{\int_A (p_T - \langle p_T \rangle_A) \langle \delta N \delta n(p_T) \rangle}{\langle N_A \rangle \langle p_T \rangle_A} \right) \\ &\approx \frac{\int_A p_T \langle n(p_T) \rangle}{\int_A \langle n(p_T) \rangle} , \end{aligned} \quad (19)$$

which implies

$$\int_A (p_T - \langle p_T \rangle_A) \langle n(p_T) \rangle = \int_A p_T \langle n(p_T) \rangle - \langle p_T \rangle_A \int_A \langle n(p_T) \rangle = 0 \quad (20)$$

Plugging Eq. (18) into Eq. (17), we obtain

$$\begin{aligned}\delta[p_T]_A &= \frac{N}{N_A} \int_A (p_T - \langle p_T \rangle_A) \delta n(p_T) \\ &\quad + \frac{\delta N}{N_A} \int_A (p_T - \langle p_T \rangle_A) \langle n(p_T) \rangle \\ &\quad - \frac{1}{N_A} \int_A (p_T - \langle p_T \rangle_A) \langle \delta N n(p_T) \rangle \\ &\approx \frac{N}{N_A} \int_A (p_T - \langle p_T \rangle_A) \delta n(p_T)\end{aligned}\quad (21)$$

the second term vanishes because of Eq. (20) and the last higher-order term is also dropped. Again, the presence of $\langle p_T \rangle_A$ is critical to ensure the similarity of this equation to Eq. (17). Eqs. 17 and 21 are valid independent of the underlying physics.

Following Ref. [22], we assume that the EbE global radial flow fluctuation controls EbE spectra fluctuation,

$$\frac{\delta n(p_T)}{\langle n(p_T) \rangle} = \frac{v_0(p_T)}{v_0} \frac{\delta[p_T]}{\langle p_T \rangle} \quad (22)$$

Plug this into Eq. (21), we obtain,

$$\begin{aligned}\frac{\delta[p_T]_A}{\langle p_T \rangle_A} &= \frac{N}{N_A \langle p_T \rangle_A} \int_A (p_T - \langle p_T \rangle_A) \delta n(p_T) \\ &= \left[\frac{N}{N_A \langle p_T \rangle_A} \int_A (p_T - \langle p_T \rangle_A) \frac{v_0(p_T)}{v_0} \langle n(p_T) \rangle \right] \frac{\delta[p_T]}{\langle p_T \rangle}\end{aligned}\quad (23)$$

Squaring this equation, averaging over events, and then using $\langle (\delta[p_T])^2 \rangle / \langle p_T \rangle^2 = v_0^2$, we obtain,

$$\frac{\langle (\delta[p_T]_A)^2 \rangle}{\langle p_T \rangle_A^2} = \left\langle \frac{N^2}{N_A^2} \right\rangle \frac{\left(\int_A (p_T - \langle p_T \rangle_A) v_0(p_T) \langle n(p_T) \rangle \right)^2}{\langle p_T \rangle_A^2}$$

from this, and use the relation

$$\langle p_T \rangle_A = \frac{\langle N \rangle}{\langle N_A \rangle} \int_A p_T \langle n(p_T) \rangle + \frac{1}{\langle N_A \rangle} \int_A p_T \langle \delta N \delta n(p_T) \rangle,$$

but ignoring $\langle \delta N \delta n(p_T) \rangle$ term, we obtain the sum rule,

$$v_{0,A} \equiv \frac{\sqrt{\langle (\delta[p_T]_A)^2 \rangle}}{\langle p_T \rangle_A} = f \times \frac{\int_A (p_T - \langle p_T \rangle_A) v_0(p_T) \langle n(p_T) \rangle}{\int_A p_T \langle n(p_T) \rangle}, \quad (24)$$

where $f^2 = \frac{\langle (N/N_A)^2 \rangle}{\langle N \rangle^2 / \langle N_A \rangle^2}$. Assuming the fluctuation of N_A comprises of a component that is fully correlated with N and a component at fixed N , then only the 2nd component contributes, and we have $f \approx 1 + \frac{\langle (\delta N_A)^2 \rangle}{2 \langle N_A \rangle^2} |_N$. The deviation of f from unity should be very small.

From this we also reach the relation that connect the v_0 calculated between two p_T ranges from Ref. [22], $v_{0,A} =$

$C_A v_0$, where

$$C_A = \frac{f \langle N \rangle}{\langle N_A \rangle \langle p_T \rangle_A} \int_A (p_T - \langle p_T \rangle_A) \frac{v_0(p_T)}{v_0} \langle n(p_T) \rangle \quad (25)$$

Note that due to condition of Eq. (20), Eqs. (24) and (25) remain valid under a constant shift $v_0(p_T) \rightarrow v_0(p_T) + c$.

B. Relating the $v_0(p_T)$ measured in two p_T ranges

In principle, the normalization of the fractional spectra can be defined in any p_T range. However, varying the choice of p_T range effectively changes the nature of global multiplicity fluctuations defined in that range, as discussed in the main text. This results in a vertical shift that adjusts the zero-crossing point of $v_0(p_T)$ of each range to its own $\langle p_T \rangle$ value. In particular, the $v_0(p_T)$ calculated in range F and R are related by a constant

$$v_{0,R}(p_T) = v_0(p_T) - s \quad (26)$$

This change of zero-crossing point ensures the basic sum rules are satisfied.

$$\int_F v_0(p_T) = 0, \int_R v_{0,R}(p_T) = 0 \quad (27)$$

Using $\langle n_R(p_T) \rangle = \langle N \rangle / \langle N_R \rangle \langle n(p_T) \rangle$, Eq. (24) are satisfied in both F and R ,

$$\begin{aligned}v_{0,A} &\equiv \frac{\int_A (p_T - \langle p_T \rangle_A) v_{0,R}(p_T) \langle n_R(p_T) \rangle}{\int_A p_T \langle n_R(p_T) \rangle} \\ &= \frac{\int_A (p_T - \langle p_T \rangle_A) (v_0(p_T) - s) \langle n(p_T) \rangle}{\int_A p_T \langle n(p_T) \rangle} \\ &= \frac{\int_A (p_T - \langle p_T \rangle_A) v_0(p_T) \langle n(p_T) \rangle}{\int_A p_T \langle n(p_T) \rangle}.\end{aligned}\quad (28)$$

The insensitivity of $[p_T]$ fluctuation to the offset in $v_0(p_T)$ strengthen our conclusion that only the p_T -dependent change of $v_0(p_T)$ is related to the collective radial flow, because its baseline value is subject to a shift dictated by global multiplicity fluctuations.

Finally, we point out that using $n(p_T)$ is more convenient than using $N(p_T)$, since Eq. (22) has to consider additional multiplicity fluctuations:

$$\frac{\delta N(p_T)}{\langle N(p_T) \rangle} \approx \frac{\delta N}{\langle N \rangle} + \frac{v_0(p_T)}{v_0} \frac{\delta[p_T]}{\langle p_T \rangle} \quad (29)$$

which complicates the expression of Eqs. (24) and (25) in terms of $v'_0(p_T)$.

-
- [1] U. Heinz and B. Schenke, (2024), [arXiv:2412.19393 \[nucl-th\]](#) .
 - [2] P. Bozek and W. Broniowski, *Phys. Rev. C* **85**, 044910 (2012), [arXiv:1203.1810 \[nucl-th\]](#) .
 - [3] R. Samanta, S. Bhatta, J. Jia, M. Luzum, and J.-Y. Ollitrault, *Phys. Rev. C* **109**, L051902 (2024), [arXiv:2303.15323 \[nucl-th\]](#) .
 - [4] U. Heinz and R. Snellings, *Ann. Rev. Nucl. Part. Sci.* **63**, 123 (2013), [arXiv:1301.2826 \[nucl-th\]](#) .
 - [5] A. Hayrapetyan *et al.* (CMS), *Rept. Prog. Phys.* **87**, 077801 (2024), [arXiv:2401.06896 \[nucl-ex\]](#) .
 - [6] ATLAS Collaboration, *Phys. Rev. Lett.* **133**, 252301 (2024), [arXiv:2407.06413 \[nucl-ex\]](#) .
 - [7] H. Appelshäuser *et al.* (NA49), *Phys. Lett. B* **459**, 679 (1999), [arXiv:hep-ex/9904014](#) .
 - [8] ALICE Collaboration, *Eur. Phys. J. C* **74**, 3077 (2014), [arXiv:1407.5530 \[nucl-ex\]](#) .
 - [9] J. Adam *et al.* (STAR), *Phys. Rev. C* **99**, 044918 (2019), [arXiv:1901.00837 \[nucl-ex\]](#) .
 - [10] S. Acharya *et al.* (ALICE), *Phys. Lett. B* **850**, 138541 (2024), [arXiv:2308.16217 \[nucl-ex\]](#) .
 - [11] M. I. Abdulhamid *et al.* (STAR), *Nature* **635**, 67 (2024), [arXiv:2401.06625 \[nucl-ex\]](#) .
 - [12] G. Aad *et al.* (ATLAS), (2025), [arXiv:2503.24125 \[nucl-ex\]](#) .
 - [13] S. Acharya *et al.* (ALICE), (2025), [arXiv:2504.04796 \[nucl-ex\]](#) .
 - [14] A. Mazeliauskas and D. Teaney, *Phys. Rev. C* **93**, 024913 (2016), [arXiv:1509.07492 \[nucl-th\]](#) .
 - [15] F. G. Gardim, F. Grassi, P. Ishida, M. Luzum, and J.-Y. Ollitrault, *Nucl. Phys. A* **1005**, 121892 (2021), [arXiv:2002.01747 \[nucl-th\]](#) .
 - [16] B. Schenke, C. Shen, and D. Teaney, *Phys. Rev. C* **102**, 034905 (2020), [arXiv:2004.00690 \[nucl-th\]](#) .
 - [17] M. Gyulassy and X.-N. Wang, *Comput. Phys. Commun.* **83**, 307 (1994), [arXiv:nucl-th/9502021](#) .
 - [18] A. Bzdak and D. Teaney, *Phys. Rev. C* **87**, 024906 (2013), [arXiv:1210.1965 \[nucl-th\]](#) .
 - [19] J. Jia, S. Radhakrishnan, and M. Zhou, *Phys. Rev. C* **93**, 044905 (2016), [arXiv:1506.03496 \[nucl-th\]](#) .
 - [20] M. Aaboud *et al.* (ATLAS), *Phys. Rev. C* **95**, 064914 (2017), [arXiv:1606.08170 \[hep-ex\]](#) .
 - [21] J. Jia, C. Zhang, and J. Xu, *Phys. Rev. Res.* **2**, 023319 (2020), [arXiv:2001.08602 \[nucl-th\]](#) .
 - [22] T. Parida, R. Samanta, and J.-Y. Ollitrault, *Phys. Lett. B* **857**, 138985 (2024), [arXiv:2407.17313 \[nucl-th\]](#) .